powders

MDPI

Article

Cu-Substituted Hydroxyapatite Powder: Mechanochemical Synthesis Using Different Copper Sources and Thermal Stability

Natalya V. Eremina [1,*], Natalia V. Bulina [1,*], Mikhail A. Mikhailenko [1,2], Olga B. Vinokurova [1], Igor Y. Prosanov [1] and Marina V. Chaikina [1]

[1] Institute of Solid State Chemistry and Mechanochemistry, Siberian Branch of Russian Academy of Sciences, Kutateladze Str. 18, Novosibirsk 630128, Russia; mikhailenko@solid.nsc.ru (M.A.M.)
[2] Budker Institute of Nuclear Physics, Siberian Branch of Russian Academy of Sciences, Acad. Lavrentieva Pr. 11, Novosibirsk 630128, Russia
* Correspondence: eremina@solid.nsc.ru (N.V.E.); bulina@solid.nsc.ru (N.V.B.)

Abstract: In this paper, we present results of a study on the possibilities of the mechanochemical synthesis of copper-substituted hydroxyapatite with the replacement of calcium cations by copper cations. During the synthesis, various reagents—sources of copper cations—were used. It was found that the nature of the carrier of the doping cation plays an important role in the formation of the structure of Cu-substituted apatite. It was established that a single-phase material forms most efficiently when copper (II) phosphate is employed; however, even this reagent did not allow the introduction of a large amount of copper into the hydroxyapatite crystal lattice. Out of 10 calcium cations in the unit cell of hydroxyapatite, no more than two could be replaced by copper cations. A further increase in the copper concentration led to the formation of an amorphous product. The degree of copper substitution in hydroxyapatite increases as the oxidation state of copper increases. The thermal stability of the hydroxyapatite with the highest degree of substitution was studied. It was shown that the presence of copper cations significantly decreases the stability of hydroxyapatite. In a temperature range of 550–750 °C, it is gradually decomposed to form a mixture of rhombohedral $Ca_{2.57}Cu_{0.43}(PO_4)_2$ and CuO. The FTIR spectrum of $Ca_{2.57}Cu_{0.43}(PO_4)_2$, which is a copper-substituted β-$Ca_3(PO_4)_2$, was first studied.

Keywords: mechanochemical synthesis; hydroxyapatite; copper; copper oxide; copper phosphate; substitution; thermal stability; tricalcium phosphate

check for updates

Citation: Eremina, N.V.; Bulina, N.V.; Mikhailenko, M.A.; Vinokurova, O.B.; Prosanov, I.Y.; Chaikina, M.V. Cu-Substituted Hydroxyapatite Powder: Mechanochemical Synthesis Using Different Copper Sources and Thermal Stability. *Powders* **2023**, *2*, 678–696. https://doi.org/10.3390/powders2040042

Academic Editor: Paul F. Luckham

Received: 25 May 2023
Revised: 3 August 2023
Accepted: 1 September 2023
Published: 8 October 2023

1. Introduction

An increase in life expectancy and in the number of injuries and diseases has increased the overall demand for scaffolds, grafts, implants, and endoprostheses. Hydroxyapatite (HA), which is an inorganic material with the chemical formula $Ca_{10}(PO_4)_6(OH)_2$, is widely used in various fields of medicine including orthopedics and dentistry [1–3] due to its chemical similarity to the inorganic components of human bone and teeth [4–8]. Stoichiometric HA with a Ca/P atomic ratio 1.67 has excellent biocompatibility, non-toxicity and osteoconductive properties [4].

Because stoichiometric HA has a low bioresorption rate and does not have antibacterial properties, appropriate substituent ions are introduced into it to impart desired characteristics [9,10]. HA structure, which has hexagonal syngony with the space group $P6_3/m$ [4], is unique in that it allows for a wide variety of substitutions and for the formation of solid solutions. In the HA lattice, all ions can be partially or completely substituted [11–14]. For calcium, both isovalent and heterovalent substitution by ions of other chemical elements are possible. When calcium cations or the phosphate group are replaced, the Ca/P ratio changes because the number of these ions decreases. To keep the ionic equilibrium in the

HA structure constant, it is necessary to comply with the stoichiometry, therefore the ratio of cations and anions should be equal to 1.67, i.e., (Ca + Me)/(P + Me) = 1.67.

Ionic substitution is a powerful tool to improve the biological performance of HA. A material with enhanced biocompatibility and bioactivity, antibacterial, antifungal and anticancer properties, with improved performance in helping to prevent osteoporosis and carrying out magnetic hyperthermia therapy can be obtained via ionic substitutions in the HA crystal lattice [11–13,15].

The authors of the review [16] have analyzed numerous literature data devoted to the biological properties of copper-containing biomaterials, including hydroxyapatite. They concluded that interest in the use of Cu as a dopant has recently been growing, which is due to the important properties of copper. Material doped with copper exhibits antibacterial, angiogenic and osteogenic properties. It was found that the materials based on Cu-substituted HA (Cu-HA) have antimicrobial activity against *S. aureus* and *E. coli* [12] and antifungal activity against different species of *C. albicans*, thus preventing inflammation when using this material in surgery [12,16,17]. In vivo investigations have shown that the low doses of copper promote the formation of micro-vessels and improve the wound-healing process [18]. Copper-doped HA also promotes osteogenic differentiation, which was proven through in vitro experiments [19]. However, some data on the Cu-HA cytotoxicity available in the literature are contradictory [12]. Thus, Jacobs et al. reported the variable copper efficiency reported in different studies, sometimes very significant, which does not allow a clear understanding of the mechanism of action of the copper ions on physiological processes [16]. The reasons for the different results of the studies may be due to the different conditions of the biological experiments, as well as to the different concentrations and methods used to prepare the material. When studying material properties, it is very important to give a complete characterization of the material, its composition and structure, in order to avoid erroneous conclusions.

In numerous studies concerning the preparation of Cu-HA, liquid-phase methods of synthesis followed by high-temperature processing of the synthesized material are mainly employed [20–22]. The need to use high-temperature treatment indicates that the introduction of the copper cation into the lattice occurs during the heat treatment; therefore, this synthesis technique can be considered as a solid-phase one, similar to that described in refs. [23–25]. According to Gomes et al. [21], during high-temperature treatment below 1100 °C, the incorporation of copper into HA is possible due to the formation of a linear O–Cu–O oxocuprate entity in the hydroxyl channel of apatite with the composition $Ca_{10}(PO_4)_6(OH)_{2-2x}Cu_xO_{2x}$, where $x < 0.1$. Heat treatment above 1100 °C allows an increase in the copper concentration up to $x \approx 0.5$ with mixed valence [26].

A lower temperature treatment of the powder obtained via the coprecipitation method was chosen by Othmani et al. to obtain Cu-HA with the composition $Ca_{10-x}Cu_x(PO_4)_6(OH)_2$ [26]. Those authors argue that with this method of synthesis, the concentration of copper in apatite can reach $x = 1.5$.

There is also a simpler solid-phase version of the synthesis of Cu-HA. Previously [27], we have shown that via mechanochemical synthesis in a planetary ball mill it is possible to obtain Cu-HA with a copper concentration up to $x = 2$ without heat treatment. In addition, using the synthesis of zinc-substituted apatite as an example, we have found that the effectiveness of the mechanochemical synthesis depends on the type of initial reagent that is the carrier of the doping cation [28]. Copper, just as zinc, is a 3D element, and therefore it is likely that in the case of HA synthesis with copper, the nature of the precursor matters too.

The purpose of this work was to investigate the influence of the different sources of copper cations on the mechanochemical synthesis of Cu-HA and to analyze the thermal stability of the as-synthesized material.

2. Materials and Methods

Mechanochemical synthesis of Cu-HA samples was carried out in an AGO-2 planetary mill [29] in two 150 mL water-cooled steel drums, with steel balls weighing 200 g and at a drum rotation speed of 1800 rpm. The weight ratio of the reaction mixture to the balls was 1:20. The duration of processing of the initial mixture in the mill was 25 min. Before the synthesis, the working zone (drums and balls) of the mill was lined with a reaction mixture of the same composition. According to atomic absorption analysis, the iron content of the samples obtained using the mechanochemical method did not exceed 0.05 wt%.

The initial components for the synthesis of Cu-HA were anhydrous calcium hydrogen phosphate $CaHPO_4$ (pure grade), calcined calcium oxide CaO (pure grade), copper, copper (II) oxide CuO (pure grade), copper (I) oxide Cu_2O (pure grade), and copper hydrogen phosphate monohydrate $CuHPO_4 \cdot H_2O$ (analytical grade).

The initial components were used in a stoichiometric ratio based on the assumption that calcium cations are replaced by copper cations in accordance with the reactions:

$$6CaHPO_4 + (4 - x)CaO + xCuO \rightarrow Ca_{(10-x)}Cu_x(PO_4)_6(OH)_2 + nH_2O \quad (1)$$

$$(6 - x)CaHPO_4 + 4CaO + xCuHPO_4 \cdot H_2O \rightarrow Ca_{(10-x)}Cu_x(PO_4)_6(OH)_2 + nH_2O \quad (2)$$

$$6CaHPO_4 + (4 - x)CaO + x/2Cu_2O \rightarrow Ca_{(10-x)}Cu_x(PO_4)_6(OH)_2 + nH_2O \quad (3)$$

$$6CaHPO_4 + (4 - x)CaO + xCu \rightarrow Ca_{(10-x)}Cu_x(PO_4)_6(OH)_2 + nH_2O \quad (4)$$

In synthesis reaction 1, the copper concentration was x = 0, 0.75, 1, 1.5, 2, or 4. For reaction 2, x was 1, 1.5, or 2. Reactions 3 and 4 were carried out only at x = 1.

Powder samples after the synthesis were investigated via X-ray diffraction (XRD) and Fourier transform infrared (FTIR) spectroscopy. For XRD, a D8 Advance diffractometer (Bruker, Karlsruhe, Germany) with CuKα radiation was utilized in the Bragg–Brentano geometry. XRD patterns were recorded at a step size of 0.02° and a counting time of 188 s per step. In situ high-temperature experiments were conducted in an XRK 900 chamber (Anton Paar, Graz, Austria) with a ceramic carrier in air atmosphere. Heating was carried out stepwise at a heating rate of 10 °C/min without exposure at a given temperature. Analysis of the phase composition was carried out in the ICDD PDF-4 powder diffraction database (2011). Refinement of unit cell parameters, crystallite size, and phase concentrations was carried out via the Rietveld method [30] in the Topas 4.2 software (Bruker). FTIR spectra were acquired on an Infralum-801 spectrometer, and tablets for the analysis were obtained by pressing samples with KBr powder.

Simultaneous thermal analysis (STA) was carried out using a STA 449 F1 Jupiter device (Netzsch, Selb, Germany) equipped with a QMS 403 C Aeolos mass spectrometer (Netzsch, Selb, Germany). STA included simultaneous detection of mass loss, differential scanning calorimetry (DSC) and registration of the evolved gas using a mass-spectrometer. The measurements were performed in a corundum crucible under an argon–oxygen mixture (80:20) at a heating rate of 10 °C/min.

The morphology of the samples was analyzed using a scanning electron microscope (SEM) 3400N (Hitachi, Tokyo, Japan) with an energy dispersive X-ray (EDX) attachment for semiquantitative element analysis.

Electron paramagnetic resonance (EPR) spectra were obtained using a Spinscan-X spectrometer (Adani, Minsk, Belarus). Spectral conditions were 9.44 GHz microwave frequency, 93,750 Hz modulation frequency, 200 mcT modulation amplitude with a time constant of 0.225 s. The microwave power varied in the 0.05–80 mW range. A ~30 mg sample was placed in an ampoule of 3 mm in diameter. The measurements were carried out at room temperature.

3. Results and Discussion

3.1. Optimal Conditions of Mechanochemical Synthesis

Figure 1 shows the diffraction patterns of the reaction mixture intended for the synthesis of a Cu-HA sample with a concentration x = 1 after mechanochemical treatment for different periods. XRD analysis revealed that in the first minutes of mechanical treatment of the reagents, calcium oxide reacted with water to form calcium hydroxide through reaction (5):

$$CaO + H_2O \rightarrow Ca(OH)_2 \quad (5)$$

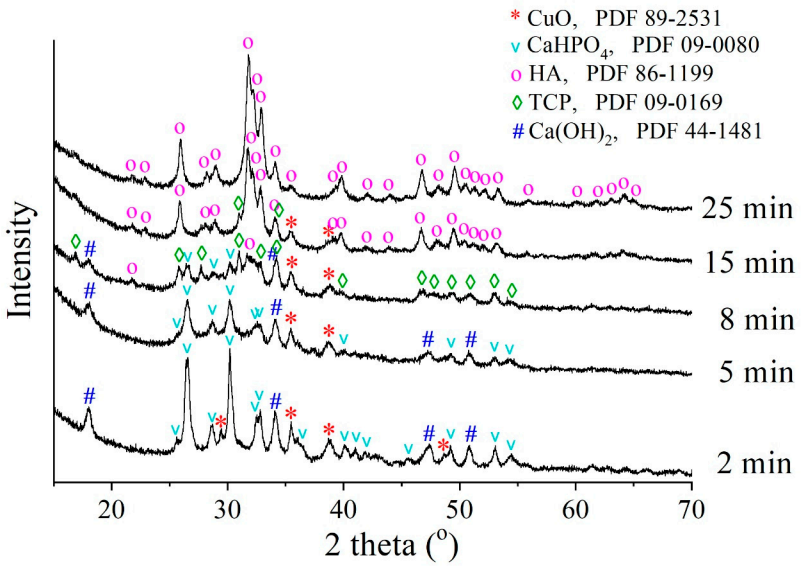

Figure 1. XRD patterns of the reaction mixture containing CuO at x = 1 after mechanochemical treatment for different periods.

After 8 min of the treatment, the concentrations of calcium hydroxide and calcium hydrogen phosphate were decreased (Figure 1) and an intermediate β-phase of $Ca_3(PO_4)_2$ (TCP) was formed. This type of calcium phosphate was also formed when preparing zinc-substituted or calcium-deficient HA via the mechanochemical method [28,31]. In both cases, the Ca/P ratio was less than 1.67. Given that only line broadening of the CuO reflections occurs, we believe that the substituent cations do not participate in the chemical reaction. The mechanical treatment only leads to a decrease in the size of CuO particles. In this case, as follows from reaction (1), the initial mixture at x = 1 has the ratio Ca/P = 1.5, which corresponds to the Ca/P ratio in $Ca_3(PO_4)_2$. Therefore, calcium hydroxide and calcium phosphate react with the formation of TCP:

$$Ca(OH)_2 + 2CaHPO_4 \rightarrow Ca_3(PO_4)_2 + 2H_2O \quad (6)$$

After 15 min of the mechanical treatment, the intensities of the reflections of both TCP and CuO phases decreased, whereas the intense reflections of the HA phase appeared. The HA phase formation is more thermodynamically favorable than TCP ($\Delta G^{TCP} = -3884$ kJ/mol, $\Delta G^{HA} = -12{,}669$ kJ/mol), consequently, the Cu-HA phase is the final product of the chemical reaction. After 25 min of the mechanical treatment, no distinct reflections of any impurity phases were detectable.

3.2. Selection of the Best Copper Source

In a comparison of samples containing different concentrations of the introduced substituent but treated for identical periods (25 min), it turned out that the concentration of the introduced copper oxide affects the degree of crystallinity of the synthesized samples (Figure 2a). The crystallinity decreased with increasing copper oxide concentration

(Table 1). Copper cations introduced into the HA lattice induce a local defect, since the Cu–O bond length is less than the Ca–O bond length, which breaks the symmetry of the unit cell and hinders the crystallite growth. An increase in the concentration of copper results in an increase in the number of defects and makes the crystallization process more difficult. At x = 4, an amorphous halo was observed in the region of the main HA reflections (2θ = 15–37°), indicating the emergence of an amorphous product. In this case, reflections of unreacted copper (II) oxide were clearly visible. Analysis of the diffraction patterns using the full-profile Rietveld method showed that reflections of the initial oxide were already present at x = 0.75 (Table 1). It is not possible to detect their presence without this method of processing diffraction patterns because reflections of CuO overlap with those of the HA phase, and at a low concentration of the oxide, its reflections are not noticeable (Figure 3). With an increase in the concentration of introduced CuO, its concentration in the synthesized products rises (Table 1), indicating that the copper oxide does not participate in the reaction with other reagents. According to the results of the quantitative analysis, when copper (II) oxide served as the initial reagent, the substitution limit could be assumed at the concentration x = 0.5.

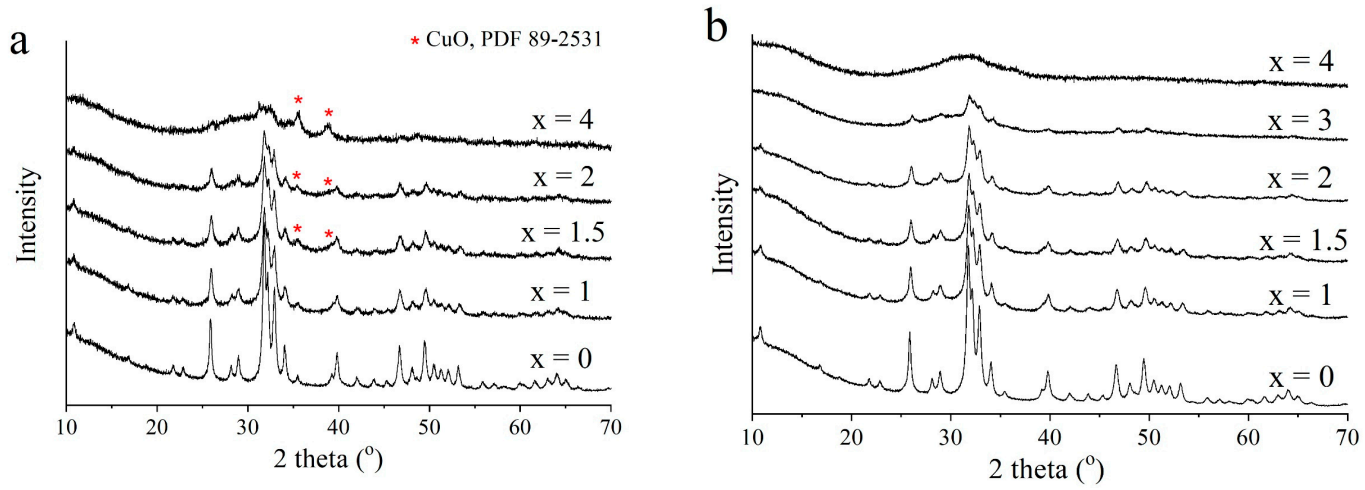

Figure 2. XRD patterns of samples containing different concentrations of initial CuO (**a**) or $CuHPO_4 \cdot H_2O$ (**b**) after mechanochemical treatment for 25 min.

Table 1. Phase composition of the synthesized samples depending on the concentration and type of copper source, as calculated via modeling of XRD patterns using the full-profile Rietveld method.

Source of Copper	x	Concentration (wt%)				Crystallinity (wt%)	R_{wp}	χ^2
		HA	CuO	Cu_2O	Cu			
CuO	0.5	100	–	–	–	98	4.3	1.2
	0.75	99.2	0.8	–	–	97	4.2	1.3
	1.0	99	1	–	–	95	4.7	1.1
	1.5	97	3	–	–	91	4.3	1.1
	2.0	95	5	–	–	83	4.2	1.1
$CuHPO_4 \cdot H_2O$	1.0	100	–	–	–	92	2.8	1.4
	1.5	100	–	–	–	86	2.2	1.1
	2.0	100	–	–	–	54	2.0	1.2
	3.0	100	–	–	–	29	1.8	1.1
Cu_2O	1.0	97	–	3	–	94	4.8	1.1
Cu	1.0	94	–	–	6	93	4.8	1.1

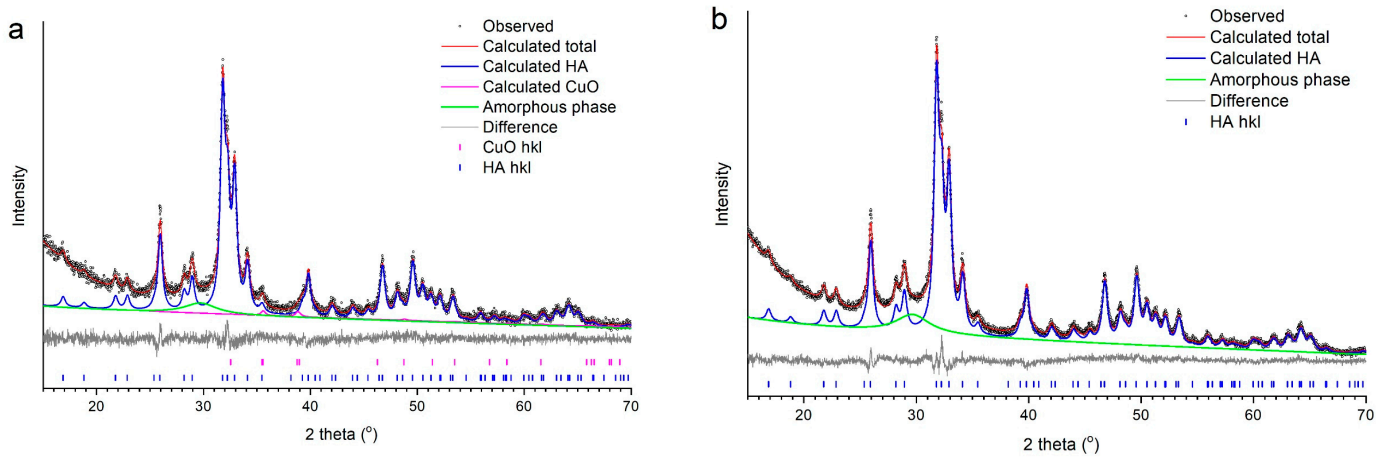

Figure 3. Full-profile Rietveld decomposition of XRD patterns of as-synthesized Cu-HA samples using CuO (**a**) and $CuHPO_4 \cdot H_2O$ (**b**) with the same copper concentration (x = 1). Duration of mechanochemical treatment for both samples was 25 min.

As presented in Figure 2b, when copper (II) orthophosphate was used, the sample remained single phase up to the concentration x = 2. Modeling using the Rietveld method also did not reveal any additional reflections of impurity phases (Figure 3, Table 1). As in the case of copper (II) oxide, when using copper (II) phosphate the intensity of reflections decreases with an increasing concentration of the introduced substituent, which indicates a decrease in the crystallinity of the sample (Figure 2b, Table 1). At x = 3, the degree of crystallinity is less than 50%. For the concentration x = 4, a fully amorphous structure is formed with a broad amorphous halo observed in the region of the most intense reflections of HA (Figure 2b). It can be assumed that in this case, the substitution of calcium for copper is realized up to x = 2.

In contrast to the use of CuO, in the case of $CuHPO_4 \cdot H_2O$ the reaction between the reagents is more efficient, which is evidently due to the presence of crystallization water (in the reagent) accelerating the interaction [32] as well as the phosphate groups surrounding the copper cation; the latter conditions should also favor the incorporation of individual components of the initial copper phosphate into the emerging Cu-HA crystal lattice. The presence of an amorphous phase at x = 4 when both sources of copper were used indicates the impossibility of the formation of a Cu-HA crystal lattice at such a concentration of copper. The copper cation is much smaller than the calcium cation; consequently, its presence in the apatite lattice at the position of calcium cations should lead to local distortions and various defects [14] that limit further growth of the crystal lattice.

Figure 4 shows the FTIR spectra of Cu-HA samples synthesized via the introduction of various concentrations of copper (II) oxide or phosphate. The spectrum of unsubstituted HA contains absorption bands of the phosphate ion (572, 602, 960, 1048 and 1090 cm^{-1}), of the hydroxyl group (630 and 3572 cm^{-1}), of the carbonate group (1420 and 1470 cm^{-1}) and of adsorbed water (wide bands at 1640 and 3500 cm^{-1}). The introduction of copper (II) as either the oxide or phosphate into HA broadens the bands belonging to the phosphate tetrahedron, thus pointing to a decrease in the crystallinity of the material as is consistent with the XRD data. The higher the concentration of copper, the wider the bands. It should be noted that in the obtained set of bond vibrations in the phosphate tetrahedron, a pronounced shift of the minimum is observed only for the band of symmetrical stretching vibration at 960 cm^{-1}, which undergoes a shift toward lower frequencies by 20 cm^{-1} for the sample with x = 2. The relative intensities of bands related to hydroxyl ions diminished (and the bands also broadened) as a function of the copper content. Similar behavior of absorption bands of the hydroxyl group has been reported by Othmani et al. [26]. Those authors explain this behavior by a decrease in crystallinity owing to the presence of copper in the HA crystal lattice. In our opinion, the most likely cause is the presence of a copper

cation in the immediate environment of the hydroxyl group (at the Ca2 site), resulting in the disruption of libration vibrations at 630 cm^{-1}. The stretching vibrations of the hydroxyl group at 3572 cm^{-1} are less pronounced in Cu-substituted samples and overlap with the wide absorption band of adsorbed water; therefore, it is quite difficult to determine whether this band disappears or only broadens after the doping.

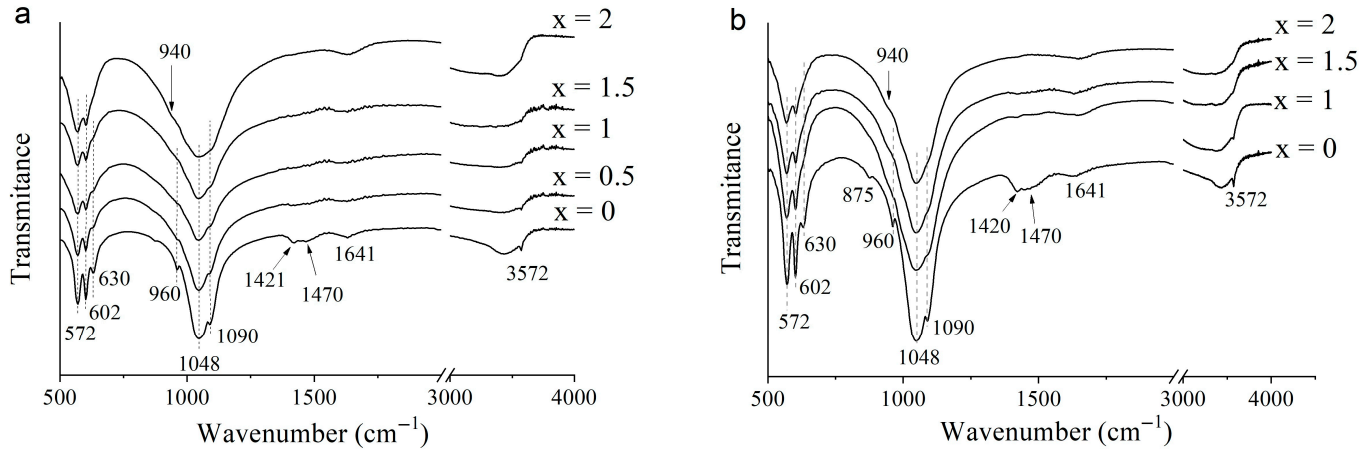

Figure 4. FTIR spectra of samples containing different concentrations of initial CuO (**a**) or $CuHPO_4 \cdot H_2O$ (**b**), after mechanochemical treatment for 25 min.

In Figure 5, one can see that unit cell parameters of the apatite phase and its volume have similar dynamics when copper (II) oxide is compared with orthophosphate, but there is a slight shift along the vertical axis. The most pronounced dependence on the substituent concentration is observed for the ***c*** parameter. An almost linear decline is seen with the increasing substituent concentration. The deviation from the linear dependence is the smallest in the case of copper phosphate. Parameters ***a*** and ***c*** for these samples are lower than those in the case of copper (II) oxide. Based on the assumption that copper cations replace calcium cations in the HA lattice, a decrease in the parameters and volume of the unit cell should take place because $r(Ca^{2+})$ = 1.00 Å and $r(Cu^{2+})$ = 0.73 Å. Consequently, when orthophosphate is used, the HA lattice contains more copper cations. The deviation from the linear dependence suggests that at high concentrations of introduced copper, not all substituent cations are incorporated into the Cu-HA lattice; consistent with the results of the quantitative analysis of samples containing copper oxide, where initial CuO was present among synthesis products (Table 1). When the orthophosphate is introduced, the residual copper that failed to become incorporated into the HA is clearly contained in the amorphous phase. Thus, we can conclude that the substitution process is the best when copper (II) orthophosphate is employed. A single-phase product can be obtained at up to x = 2.0. Nevertheless, probably not all the introduced copper is located in the HA lattice in this case.

Next, the use of copper sources with Cu charges +1 and 0 at the concentration x = 1 was evaluated. In Figure 6a, one can see that when Cu_2O or metallic copper was applied as the initial source 100% conversion was not observed either. Rietveld refinement of the XRD patterns revealed the initial reagents in both cases (Figure 7). However, no additional absorption bands are seen in the FTIR spectra of these samples (Figure 6b), because the vibrations of Cu–O bonds lie outside of the studied range. The spectra of all samples were identical.

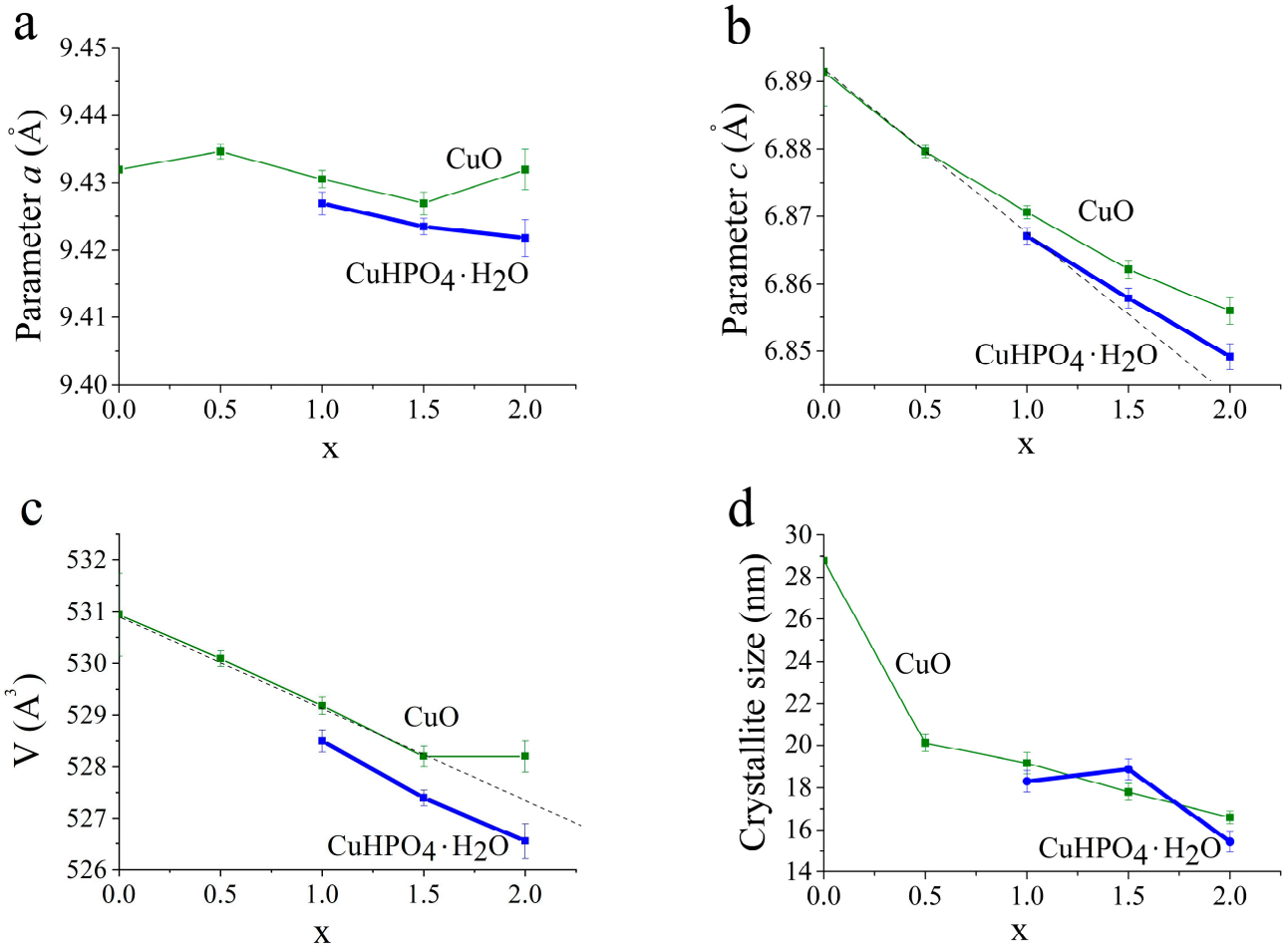

Figure 5. Changes in parameters *a* (**a**) and *c* (**b**) of the HA unit cell, volume (**c**), and crystallite size (**d**) with an increase in the concentration of the initial CuO or $CuHPO_4 \cdot H_2O$.

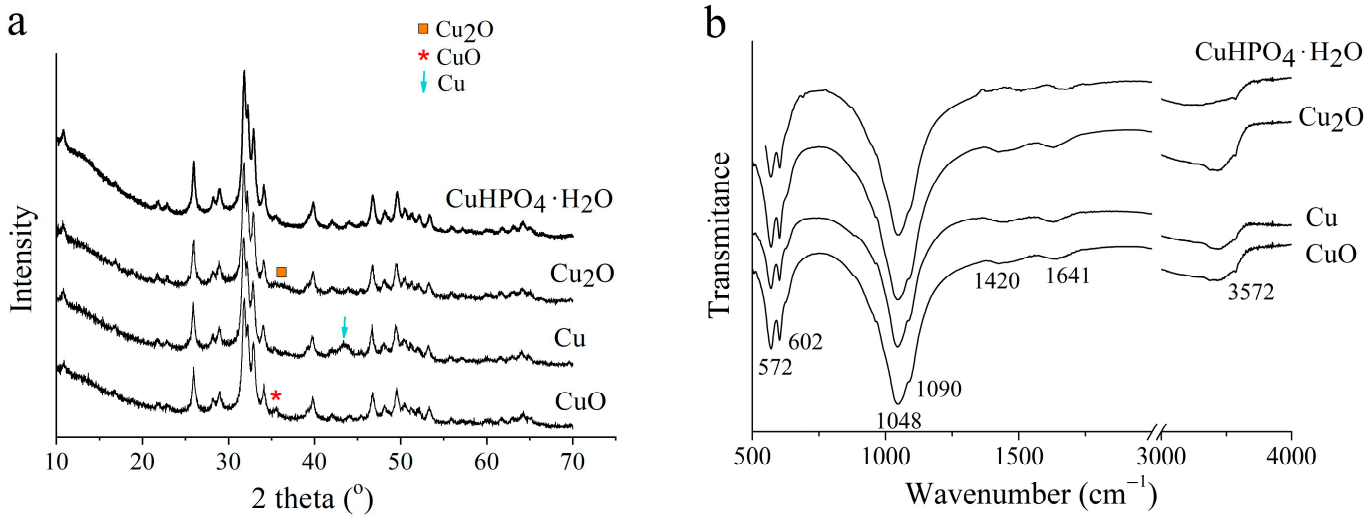

Figure 6. XRD patterns (**a**) and FTIR spectra (**b**) of Cu-HA samples with different sources of Cu at x = 1 and mechanochemical treatment for 25 min.

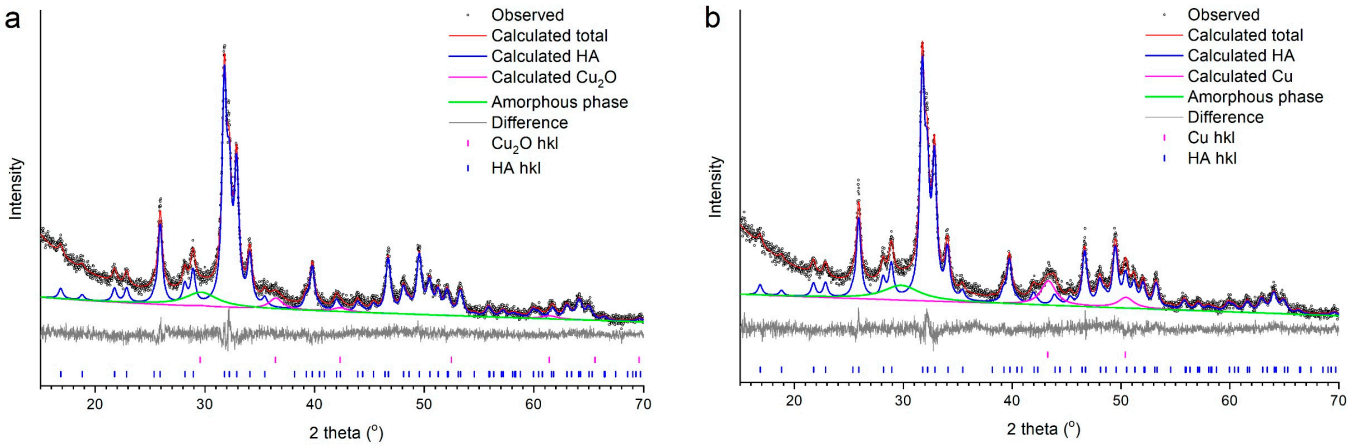

Figure 7. Full-profile Rietveld refinement of XRD patterns of Cu-HA samples synthesized using Cu_2O (**a**) and Cu (**b**) at concentration x = 1. Duration of mechanochemical treatment for both samples is 25 min.

When comparing lattice parameters of the HA phase obtained by the introduction of identical concentrations of copper from different initial reagents (Figure 8a,b), one can see that the lowest unit cell parameters are obtained with copper (II) phosphate; therefore, the synthesis is the most efficient when this reagent is used. The same is true for unit cell volume (Figure 8c). Crystallite size is approximately the same among samples synthesized from different sources of copper and is significantly less than that of unsubstituted HA (Figure 8d). Therefore, the insertion of copper in the form of any initial reagent complicates the process of HA lattice formation.

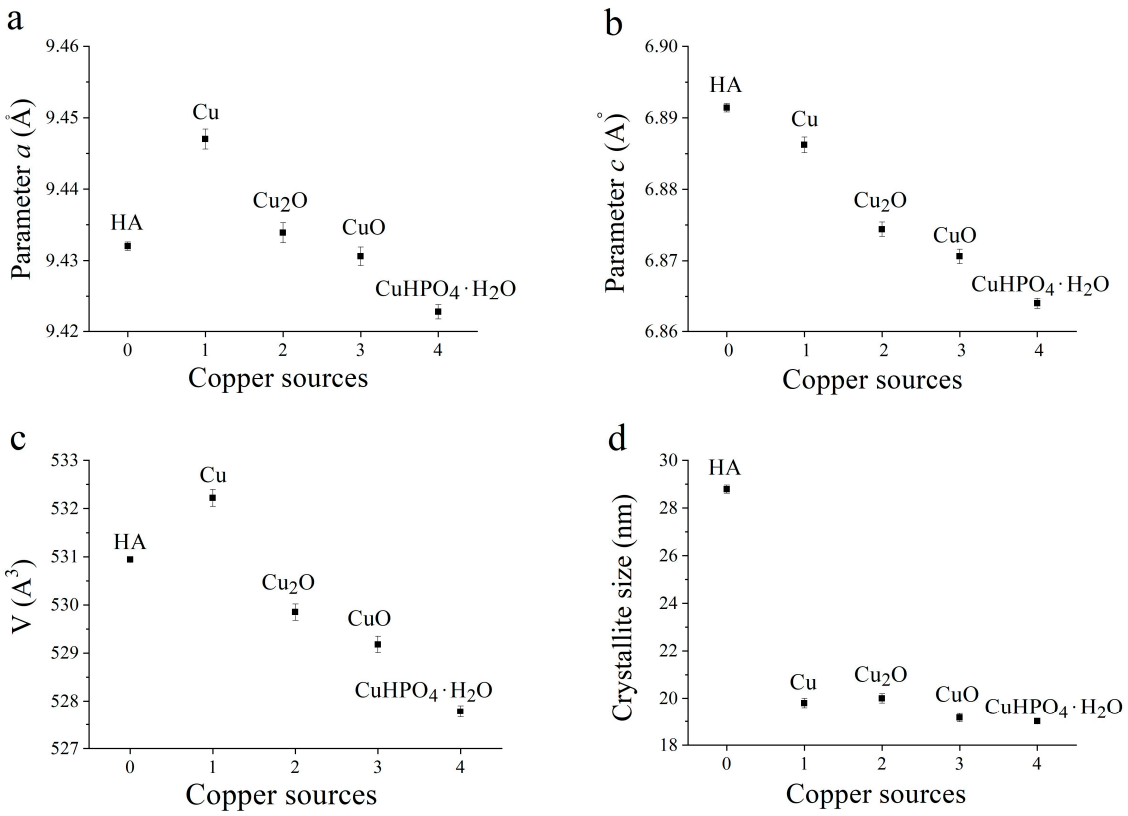

Figure 8. A comparison of unit cell parameters *a* (**a**) and *c* (**b**), cell volume (**c**), and crystallite size (**d**) in Cu-HA for syntheses from different copper sources at concentration x = 1. Duration of mechanochemical treatment for all the samples is 25 min.

As seen in Figure 9, the concentrations of copper in all the samples are approximately the same and correspond to the theoretical value (10.4% wt.) introduced according to the reaction stoichiometry given by Equations (1)–(4) for x = 1. Since all the samples have the same copper concentration and they were treated in the same reaction conditions, the difference in their lattice parameters (Figure 8) is attributed to different amount of copper in the apatite lattice.

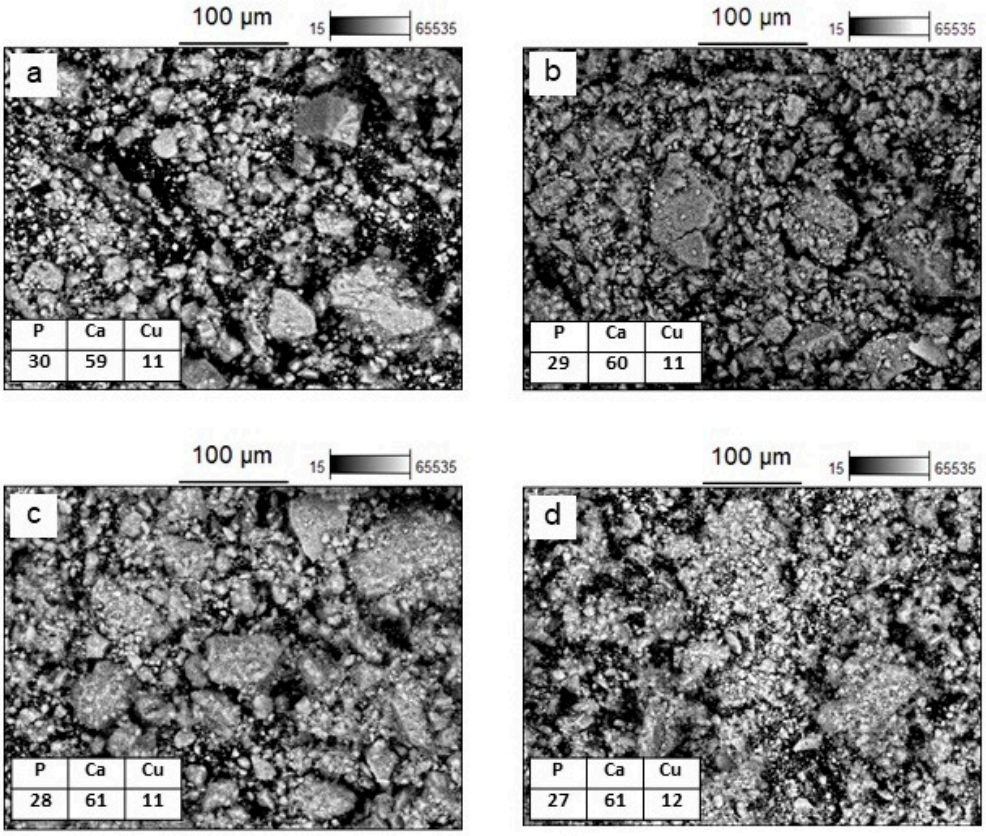

Figure 9. SEM images of powder morphology of the Cu-HA samples synthesized using CuO (**a**), $CuHPO_4 \cdot H_2O$ (**b**), Cu_2O (**c**) and Cu (**d**) at concentration x = 1. Duration of mechanochemical treatment for all samples is 25 min. The tables show the weight concentrations of the registered elements at the semiquantitative EDX analysis of these areas.

The EPR spectra of the studied samples (Figure 10) are similar to those reported in previous work on Cu-HA [33]. There are at least two signals with g = 2.45 and 2.17 corresponding to the Cu^{2+} ions [33]. The different values of the g-factors are due to the different local environments of the copper cations. If we assume that copper cations are localized in the positions of calcium cations (see reactions 1–4), then there are two non-equivalent Ca sites in the HA (Ca1 and Ca2) with different local environments, which can be replaced by the substituent. However, in order to prove this assumption, further studies are needed. For the sample obtained using metallic copper as the initial reagent, the EPR signal shape is slightly different (Figure 10). The reason for this can be attributed to the presence of metallic copper in the final sample (Table 1), due to which its sintering occurs during the EPR measurements. As seen in Figure 10, when Cu(I) and Cu(0) are used as the initial reagents, a part of copper is oxidized to Cu(II) during mechanochemical synthesis. Copper, most likely, is incorporated into the HA lattice only in the Cu^{2+} state.

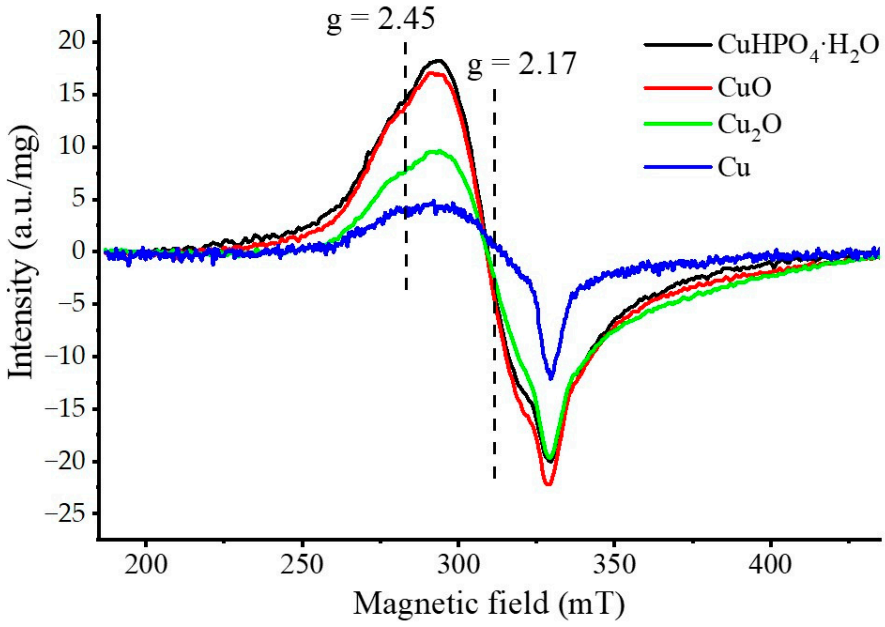

Figure 10. EPR spectra of the samples synthesized using different copper sources at concentration x = 1. Microwave power is 0.5 mW.

For all the Cu-HA samples, the change in the power of the supplied microwave radiation did not change the EPR spectra (Figure 11). Figure 12 shows the integral intensities of the EPR signal of the as-synthesized samples and the reference sample $CuCl_2 \cdot 2H_2O$ as a function of the microwave power. As seen, in all cases, the EPR signal does not reach a plateau level when increasing the microwave power up to 80 mW, indicating very short relaxation times, which is characteristic of copper.

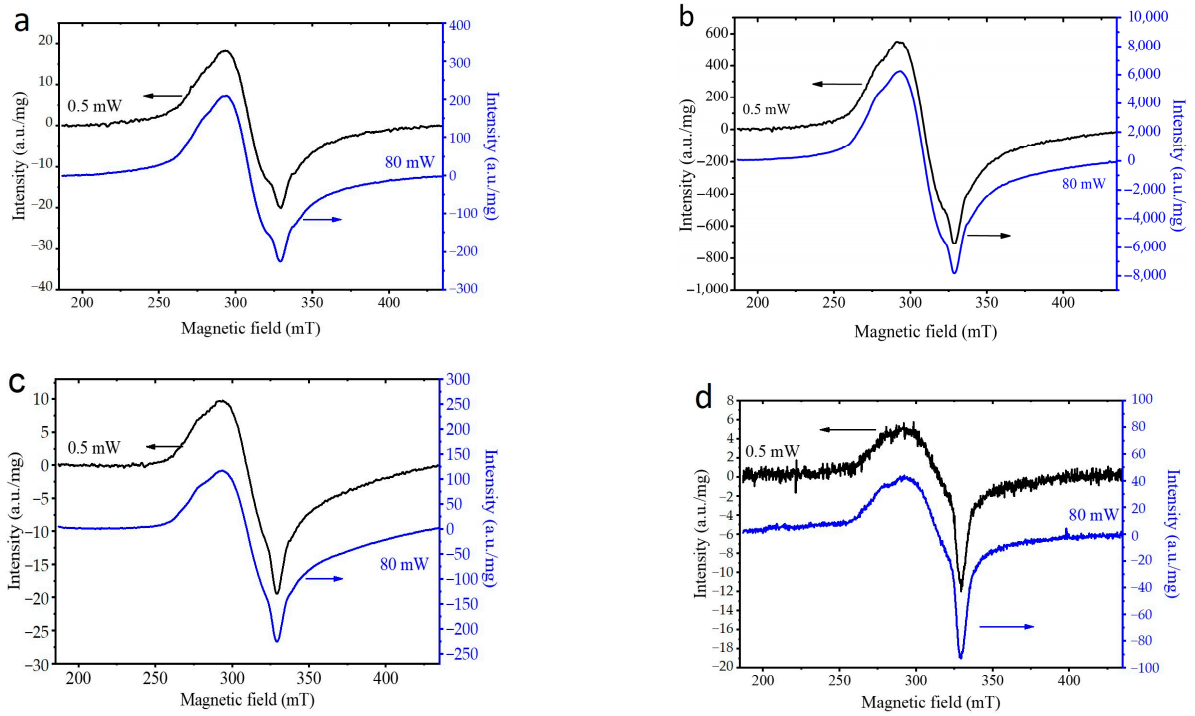

Figure 11. EPR spectra of the samples synthesized using $CuHPO_4 \cdot H_2O$ (**a**), CuO (**b**), Cu_2O (**c**) and Cu (**d**) at x = 1, at different powers of microwave irradiation.

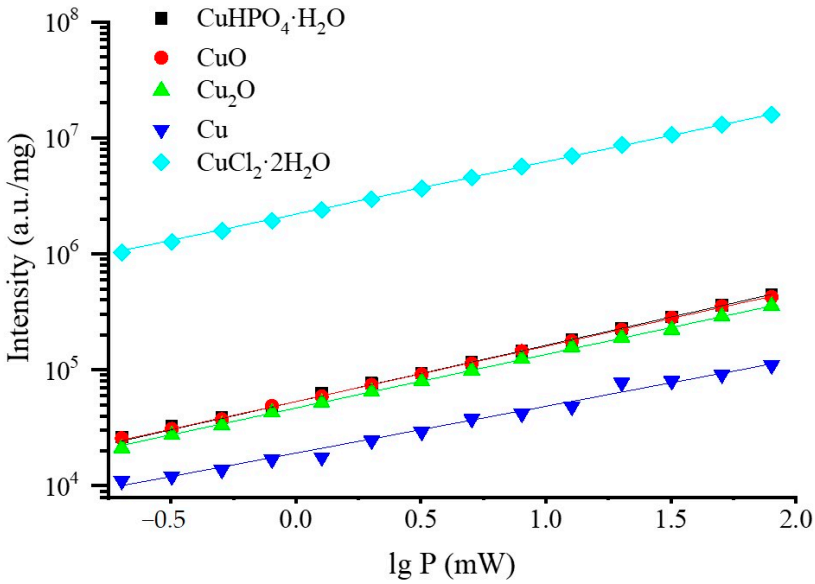

Figure 12. Integral intensities of the EPR signal of $CuCl_2 \cdot 2H_2O$ and the samples synthesized using different copper sources (x = 1) as a function of the power of microwave irradiation.

Table 2 presents the data derived by extrapolating the values from Figure 12, using the equation for exponential growth of the signal intensity with the increasing power of microwave radiation:

$$I = I_0 + Ae(x/t) \quad (7)$$

Table 2. The values of the slopes (t) of the lines defined by Equation (7) calculated from the data given in Figure 12.

Sample	t
Cu-HA from $CuHPO_4 \cdot H_2O$	0.8929 ± 0.005
Cu-HA from CuO	0.91044 ± 0.008
Cu-HA from Cu_2O	0.93951 ± 0.012
Cu-HA from Cu	1.07505 ± 0.052
$CuCl_2 \cdot 2H_2O$	0.95962 ± 0.006

For all the synthesized samples, the t values are close to that for $CuCl_2 \cdot 2H_2O$, which is usually used as the reference sample for EPR measurements (Table 2). The higher value for the sample prepared using metallic copper may be caused by heating of the sample during the measurement.

The dependence of the logarithm of the integrated intensity of the EPR signal on the degree of copper conversion shows (Figure 13) that there is a correlation between the XRD and EPR data. The more copper that has reacted in the process of mechanochemical synthesis, the more Cu^{2+} cations are incorporated into the apatite structure. There are no data for the sample doped with metallic copper in Figure 13, because when heated during the measurements at a high microwave power, sintering of the sample occurred. High temperature, most likely, induced structural changes in the sample, which caused the data obtained to deviate significantly from those of the other samples.

From the above, it can be concluded that the type of the initial reagent that is the carrier of the substituent cation in mechanochemical synthesis is of great importance for the synthesis of Cu-HA. Among the possible valence states of copper, the most efficient synthesis occurs with the divalent state, and it is better to use copper phosphate than oxide.

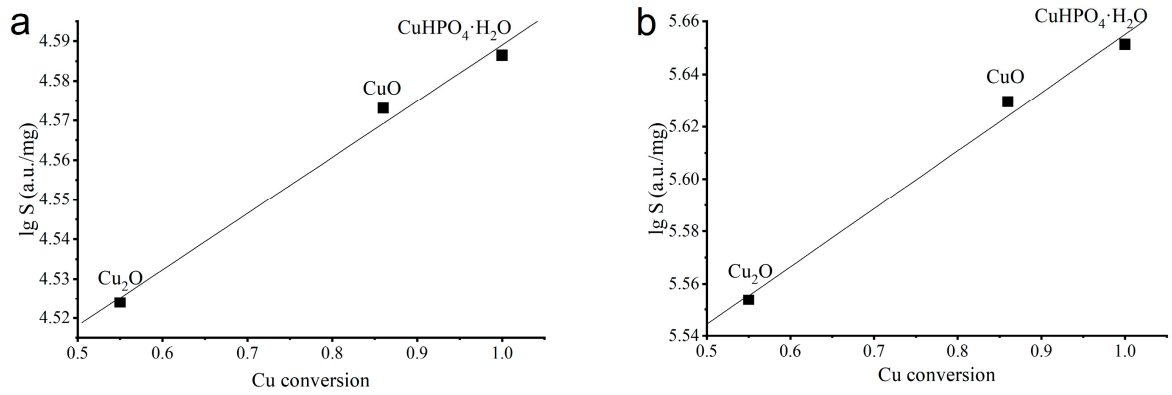

Figure 13. Decimal logarithm of the integral intensity of the EPR signal (lg S) at 0.5 mW (**a**) and 80 mW (**b**) on the degree of copper conversion according to XRD data (Table 1).

3.3. Thermal Stability of Cu-Substituted Hydroxyapatite

The thermal stability of Cu-HA was studied for the sample with a maximum concentration of the copper cation in the apatite structure, according to XRD analysis, namely, for the $CuHPO_4 \cdot H_2O$ sample with the substitute content x = 2. The STA data presented in Figure 14a show that when the sample was heated up to 1000 °C, a mass loss of 7.5 wt% occurred. The mass spectrometry data indicate that the main mass loss is caused by the release of water occurring in several steps (Figure 14a). The removal of adsorbed water is observed up to 250 °C and has a maximum release at 146 °C. Next, the release of lattice water with a maximum at 245 °C occurs up to 600 °C. The DSC curve of the sample exhibits an exo-effect at 615 °C, which is not accompanied by water release. According to our earlier study of the sample Cu-HA with substitute content x = 0.5 [34], we can assume that at this temperature the release of copper oxide may occur, followed by the formation of the second impurity phase, β-tricalcium phosphate $Ca_3(PO_4)_2$ (β-TCP), which has a rhombohedral structure with the space group *R*3*c*. Both of these phases are formed upon the decomposition of Cu-HA. In order to confirm this assumption, the phase composition of the samples heated up to 640 °C first and then to 1000 °C has been studied.

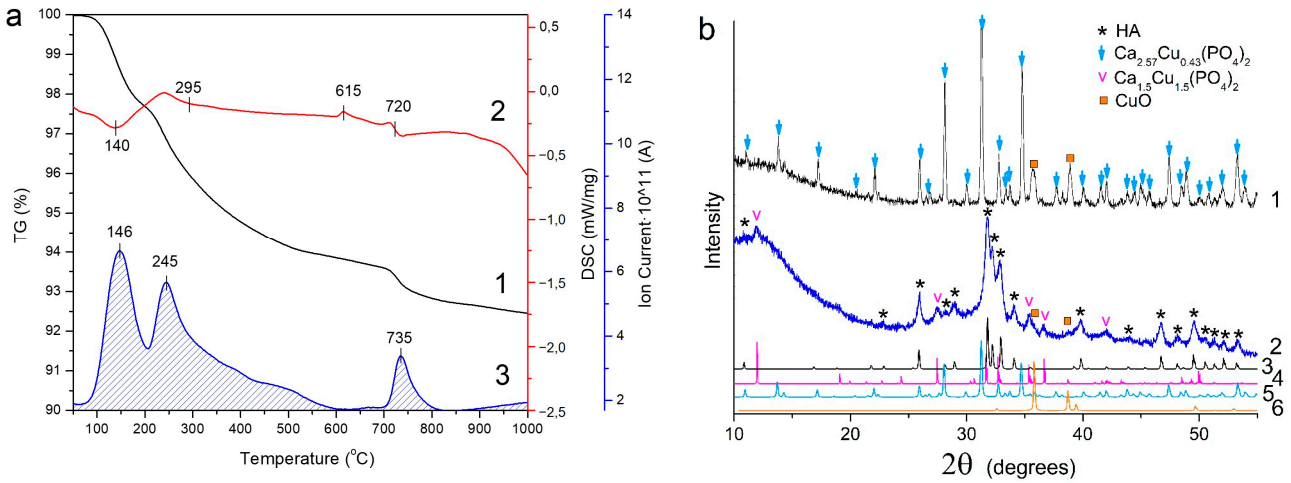

Figure 14. STA (**a**) of Cu-HA sample with copper phosphate content x = 2; 1—mass loss; 2—DSC; 3—evolution of water. XRD patterns (**b**) of the sample after STA upon heating up to 1000 °C (1) and 640 °C (2) in comparison with modeled patterns from the PDF database: 3—HA, PDF 000-86-1199; 4—$Ca_3Cu_3(PO_4)_4$, PDF 000-72-0203; 5—$Ca_{18}Cu_3(PO_4)_{14}$, PDF 000-53-0171; 6—CuO, PDF 000-89-2531.

Figure 14b shows the XRD patterns of the samples so obtained. As seen, the decomposition of the copper-substituted apatite with x = 2 does not occur in the same way as in

the case with x = 0.5 [34]. Thus, upon heating of the sample to a temperature of 640 °C, the $Ca_3Cu_3(PO_4)_4$ phase which has a monoclinic symmetry with the space group $P2_1/a$ (PDF 000-72-0203) is formed. The sample also contains a small amount of copper(II) oxide (Figure 14b). After heating the sample to 1000 °C, it does not contain the apatite phase; there is a mixture of CuO and phosphate, the lattice parameters of which are close to $Ca_{18}Cu_3(PO_4)_{14}$ with the rhombohedral space group *R*3*c* (PDF 000-53-0171). The composition of both orthophosphates can be given as $Ca_{3-x}Cu_x(PO_4)_2$. In this case, the monoclinic and rhombohedral modifications should have the compositions $Ca_{1.5}Cu_{1.5}(PO_4)_2$ and $Ca_{2.57}Cu_{0.43}(PO_4)_2$, respectively. From this it follows that an increase in temperature leads to a decrease in the copper content in the orthophosphate $Ca_{3-x}Cu_x(PO_4)_2$, and therefore the concentration of the CuO phase increases. The phase composition of the as-prepared samples determined from Rietveld X-ray refinements are given in Table 3.

Table 3. Phase composition of the synthesized samples after heating in different conditions.

Type of Experiment	Temperature (°C)	Concentration (wt%)			
		Cu–HA	$Ca_{1.5}Cu_{1.5}(PO_4)_2$ (Monoclinic)	$Ca_{2.57}Cu_{0.43}(PO_4)_2$ (Rhombohedral)	CuO
STA measurement	640	86	13	–	>1
	1000	–	–	91	9
In situ diffraction	550	86	7	7	–
	650	47	5	42	12
	800	–	–	93	7
Heating in the furnace	500	100	–	–	–
	600	76	22	–	3
	800	–	–	92	8
	1000	–	–	92	8

Thus, it can be concluded that the phase transition observed at 615 °C corresponds to the partial decomposition of the substituted apatite with the formation of phosphate $Ca_{1.5}Cu_{1.5}(PO_4)_2$ of a monoclinic modification. At 720 °C, the complete decomposition of the apatite phase occurs with a change of the monoclinic structure of $Ca_{1.5}Cu_{1.5}(PO_4)_2$ to the rhombohedral structure of $Ca_{2.57}Cu_{0.43}(PO_4)_2$ with a low content of copper. As a result, the concentration of copper (II) oxide in the sample increases.

It should be noted that the exo-process at 615 °C is not accompanied by the release of water (Figure 14b), although during the transformation of the Cu-HA structure, containing a hydroxyl group, into $Ca_{1.5}Cu_{1.5}(PO_4)_2$ it should be released. One possible reason why water is not released is the presence of the H-$(PO)_4$ group or hydrated water in the structure of the released phosphate. Ruszala and Kostiner [35] reported the formation of the $Ca_{18}Cu_2H_2(PO_4)_{14}$ compound, whose chemical formula can be given as $Ca_{2.57}Cu_{0.29}H_{0.29}(PO_4)_2$, which indicates a possibility of the existence of compounds of the $Ca_{3-x}Cu_{x-x/2}H_{x/2}(PO_4)_2$ type. The rearrangement of the $Ca_{3-x}Cu_{x-x/2}H_{x/2}(PO_4)_2$ structure into a mixture of $Ca_{2.57}Cu_{0.43}(PO_4)_2$ and CuO upon heating will lead to the release of H_2O, which was observed in our case at 720 °C (see Figure 14b).

In situ diffractometric studies showed that the process of high-temperature structural transformation of Cu-HA depends on the heating conditions. Figure 15a shows how the composition of the sample changes during heating in a high-temperature diffractometer chamber. It should be noted that in this case, the heating rate was equal to that for the STA experiments, but the heating process had to be stopped during recording of the patterns. As a result, the sample was kept for 15 min at a given temperature. In addition, in this experiment, the sample was placed on a flat thin corundum plate, which allowed rapid uniform heating of the entire volume of the sample. These slightly different conditions for heating the material probably resulted in an earlier decomposition of the Cu-HA phase. Thus, at 550 °C, in the in situ experiment, the simultaneous presence of the apatite phase with the phosphates $Ca_{1.5}Cu_{1.5}(PO_4)_2$ and $Ca_{2.57}Cu_{0.43}(PO_4)_2$ was observed (Figure 15a).

At 650 °C, the content of $Ca_{2.57}Cu_{0.43}(PO_4)_2$ significantly increases due to a decrease in the apatite content. Apart from that, copper (II) oxide is also formed. At 800 °C, only two phases are observed, such as $Ca_{2.57}Cu_{0.43}(PO_4)_2$ and CuO, which agree with the composition of the sample after STA upon heating to 1000 °C (Table 3).

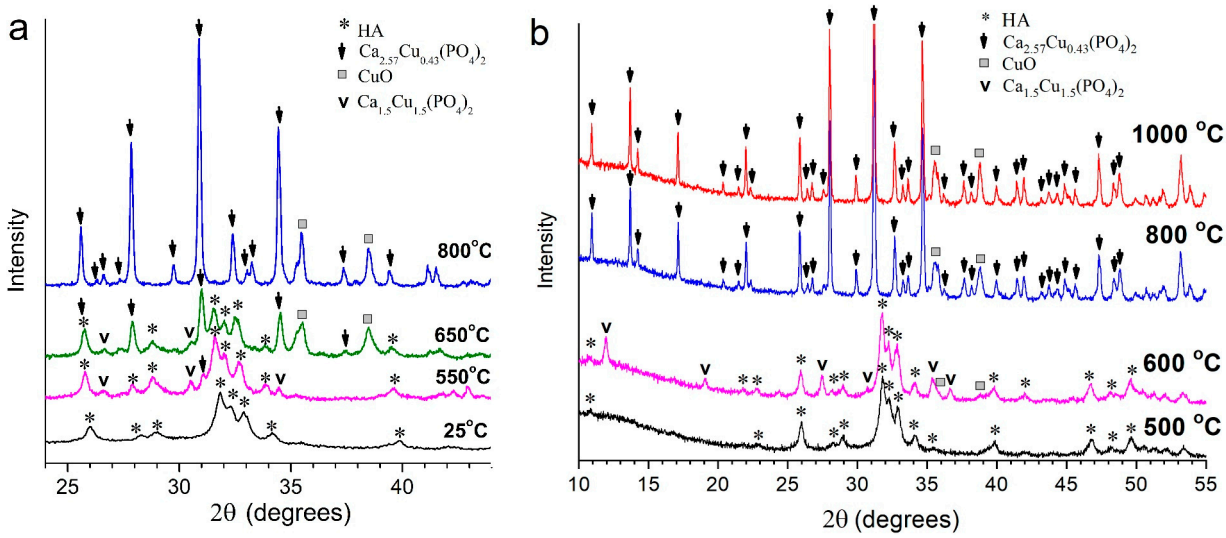

Figure 15. In situ (**a**) and ex situ (**b**) XRD patterns of Cu-HA sample, synthesized with cupper phosphate content x = 2.

Upon heating the Cu-HA sample with x = 2 in a high-temperature furnace in a corundum crucible, at storage, at a given temperature for 2 h followed by cooling, the formation of the same phases as in the case of STA experiments, carried out in a corundum crucible, was observed. When heated, the sample in a high-temperature furnace at prolonged storage (2 h) at a given temperature is stable up to 500 °C (Figure 15b). After heating at 600 °C, the $Ca_{1.5}Cu_{1.5}(PO_4)_2$ and CuO phases are released in the sample. Exposure at 800 °C leads to complete decomposition of the apatite phase and disappearance of the reflections attributed to $Ca_{1.5}Cu_{1.5}(PO_4)_2$. Only $Ca_{2.57}Cu_{0.43}(PO_4)_2$ and CuO phases are observed (Figure 15, Table 3). As seen, the phase composition of the sample does not change as the temperature increases up to 1000 °C.

Figure 16 shows the FTIR spectra of the samples heat-treated in a high-temperature furnace. It can be seen that for the sample heated above 500 °C, there are only the absorption bands attributed to hydroxyapatite [4], which is consistent with the phase composition of this sample (Table 3). The bending vibrations of the O-P-O bond (569 and 602 cm^{-1}), the stretching vibrations of the P-O bond (962, 1044 and 1088 cm^{-1}), and the libration (630 cm^{-1}) and stretching (3570 cm^{-1}) vibrations of the OH group are observed (Figure 16). After heating above 600 °C, an absorption band at 630 cm^{-1} belonging to the libration vibrations of the OH group significantly increases, while the intensity of the stretching vibrations of the OH group at 3570 cm^{-1} do not change. This is consistent with the X-ray phase analysis (Table 3), indicating the partial decomposition of Cu-HA with the formation of the copper-containing phase upon the heating of the sample at 600 °C. Obviously, a large part of the copper passes from Cu-HA to the phosphate $Ca_{1.5}Cu_{1.5}(PO_4)_2$. The copper cations located in the Cu-HA crystal lattice in the position of calcium cations at 500 °C disrupt the local environment of the hydroxyl groups and dampen the librational vibrations of the OH group. The same behavior has been reported for Sr-substituted HA [36]. When the Cu-HA unit cells containing copper cations are transformed into $Ca_{1.5}Cu_{1.5}(PO_4)_2$ phosphate, the remaining apatite contains only the calcium cations, so the local environment of all the hydroxyls at 600 °C becomes symmetric again and the intensity of the absorption bands of the libration vibrations increases.

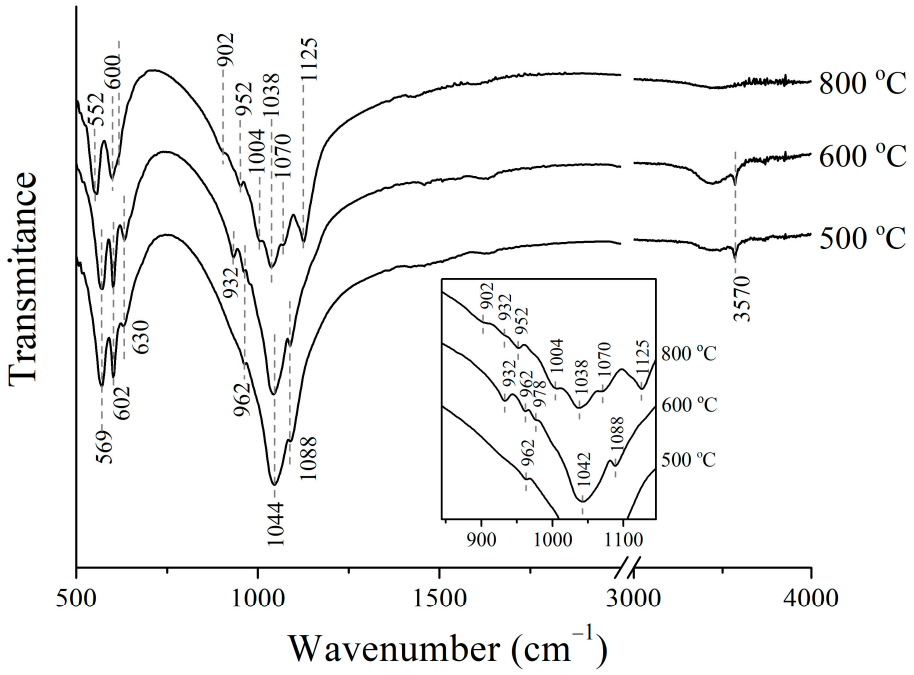

Figure 16. FTIR spectra of the heated Cu-HA samples with copper phosphate content x = 2.

It is worth noting that the FTIR spectrum of the sample obtained at 600 °C (Figure 16) also contains low-intensity absorption bands at 932 and 978 cm^{-1}, which we attributed to the vibrations of the phosphate group in $Ca_{1.5}Cu_{1.5}(PO_4)_2$, whose content in the sample is 22 wt% (Table 3).

Based on the data given in Table 3, it can be assumed that the absorption bands observed in the FTIR spectrum of the sample heated above 800 °C (Figure 16) belong to the vibrations of the phosphate group of $Ca_{2.57}Cu_{0.43}(PO_4)_2$. This spectrum is similar to that of the unsubstituted $Ca_3(PO_4)_2$ of a rhombohedral modification as in the case of $Ca_{2.57}Cu_{0.43}(PO_4)_2$, however, the position and number of bands in the spectra are different [31,37,38]. Figure 16 shows that the FTIR spectrum of the $Ca_{2.57}Cu_{0.43}(PO_4)_2$ sample heated above 800 °C is similar to that of the Cu-HA sample heated above 500 °C. Taking this into account, one may suggest that the bands at 552 and 600 cm^{-1} in the spectrum of $Ca_{2.57}Cu_{0.43}(PO_4)_2$ belong to the bending vibrations of the O-P-O bond, whereas the bands observed in the 900–1200 cm^{-1} range can be attributed to the stretching vibrations of the P-O bond. Unlike the unsubstituted $Ca_3(PO_4)_2$, for $Ca_{2.57}Cu_{0.43}(PO_4)_2$ a large number of bands are observed in the 900–1200 cm^{-1} range, which are due to the different local environments of the tetrahedral phosphate ions in $Ca_{2.57}Cu_{0.43}(PO_4)_2$.

In summary, we can conclude that, unlike stoichiometric HA, which is stable up to 1300 °C [39], Cu-HA with x = 2 is stable up to ~500 °C. This temperature is 200 °C lower than that reported by Bulina et al. [34] for Cu-HA with x = 0.5. Apparently, the thermal stability of Cu-HA depends on the concentration of the introduced substituent cation. The higher the substituent concentration, the lower the thermal stability of the material. At substituent content x = 2, the decomposition of Cu-HA begins with the formation of copper-containing phases $Ca_{3-x}Cu_x(PO_4)_2$ and CuO. At a temperature of ~720 °C, complete decomposition of Cu-HA results in the formation of the rhombohedral $Ca_{2.57}Cu_{0.43}(PO_4)_2$ and CuO mixture.

4. Conclusions

A study on the mechanochemical synthesis of Cu-HA from various sources of copper (Cu, CuO, Cu_2O, or $CuHPO_4 \cdot H_2O$) was conducted. It was found that when calcium cations are replaced by copper cations, the volume of the unit cell diminishes due to smaller parameters *a* and *c*, in agreement with the change in ionic radii after the substitution. It was

demonstrated that the charge state of the initial substituent cation is of great importance. Thus, metallic copper is the least efficient source of copper because copper, mainly in Cu (II) form, is incorporated into the apatite lattice. When the initial reagents with copper (I) and copper (0) are used in mechanochemical synthesis, a part of the copper is oxidized to Cu(II). An increase in the amount of the copper-containing compound introduced into the reaction increases the concentration of copper incorporated as Cu^{2+} ions into the HA lattice. A comprehensive study of the synthesized samples indicates that copper cations occupy two nonequivalent positions in the hydroxyapatite lattice, most likely Ca1 and Ca2. The synthesis of Cu-HA from copper (II) phosphate is the most efficient. This option makes it possible to implement the complete conversion of the initial reagents into the target product and bring the concentration of copper in apatite to x = 2. With a further increase in copper concentration, an amorphous phase arises, suggestive of a limit of the achievable substitution degree.

The Cu-HA with the highest degree of substitution (x = 2) was shown to be sensitive to heating conditions and to have low thermal stability. In the temperature range of 550–620 °C, depending on the heating conditions, the partial decomposition of Cu-HA with the formation of copper-containing phases occurs. The complete decomposition of Cu-HA is observed at ~720 °C. After heating at this temperature, the sample mainly consists of the $Ca_{2.57}Cu_{0.43}(PO_4)_2$ phase containing 8 wt% CuO.

The low thermal stability of Cu-HA prevents it from being used in high-temperature processes and for the manufacture of ceramic materials therefrom. Nevertheless, this material can be used to produce polymer composites or can be used directly if thermally treated at temperatures below 500 °C.

Author Contributions: Conceptualization, M.V.C.; methodology, N.V.B.; investigation, N.V.E., I.Y.P., M.A.M. and O.B.V.; writing—original draft preparation, N.V.E.; writing—review and editing, M.V.C. and N.V.B. All authors have read and agreed to the published version of the manuscript.

Funding: This research was carried out within the State Assignment to the Institute of Solid State Chemistry and Mechanochemistry SB RAS (project No. 121032500064-8).

Institutional Review Board Statement: Not applicable.

Informed Consent Statement: Not applicable.

Data Availability Statement: The processed data required to reproduce these results are included in the Materials and Methods section. Raw data are available upon request.

Conflicts of Interest: The authors declare no conflict of interest. The funders had no role in the design of the study; in the collection, analyses, or interpretation of the data; in the writing of the manuscript; or in the decision to publish the results.

References

1. Mucalo, M. *Hydroxyapatite (HAp) for Biomedical Applications*; Woodhead Publishing Series in Biomaterials; Woodhead Publishing: Cambridge, UK, 2015.
2. Thirumalai, J. *Hydroxyapatite: Advances in Composite Nanomaterials, Biomedical Applications and Its Technological Facets*; Intech Open: London, UK, 2018.
3. Kumar, A.; Kargozar, S.; Baino, F.; Han, S. Additive Manufacturing Methods for Producing Hydroxyapatite and Hydroxyapatite-Based Composite Scaffolds: A review. *Front. Mater.* **2019**, *6*, 313. [CrossRef]
4. Elliott, J.C. *Structure and Chemistry of the Apatites and Other Calcium Orthophosphates*; Elsevier Science: Amsterdam, The Netherlands, 1994.
5. Dorozhkin, S.V. Calcium orthophosphate ($CaPO_4$)-based bioceramics: Preparation, properties, and applications. *Coatings* **2022**, *12*, 1380. [CrossRef]
6. Okada, M.; Matsumoto, T. Synthesis and modification of apatite nanoparticles for use in dental and medical applications. *Jpn. Dent. Sci. Rev.* **2015**, *51*, 85–95. [CrossRef]
7. Azari, A.; Nikzad, S.; Yazdani, A.; Atri, F.; Anvari-Yazdi, A.F. Deposition of crystalline hydroxyapatite nano-particle on zirconia ceramic: A potential solution for the poor bonding characteristic of zirconia ceramics to resin cement. *J. Mater. Sci. Mater. Med.* **2017**, *28*, 111. [CrossRef]

8. Yang, X.; Tian, Z.; Guo, K.; Lu, T.; Ji, J. Preparation and mechanism of hydroxyapatite hollow microspheres with different surface charge by biomimetic method. *J. Mater. Sci. Mater. Med.* **2020**, *31*, 47. [CrossRef]
9. Ressler, A.; Žužić, A.; Ivanišević, I.; Kamboj, N.; Ivanković, H. Ionic substituted hydroxyapatite for bone regeneration applications: A review. *Open Ceram.* **2021**, *6*, 100122. [CrossRef]
10. Lu, J.; Yu, H.; Chen, C. Biological properties of calcium phosphate biomaterials for bone repair: A review. *RSC Adv.* **2018**, *8*, 2015–2033. [CrossRef]
11. Supova, M. Substituted hydroxyapatites for biomedical applications: A review. *Ceram. Int.* **2015**, *41*, 9203–9231. [CrossRef]
12. Tite, T.; Popa, A.-C.; Balescu, L.M.; Bogdan, I.M.; Pasuk, I.; Ferreira, J.M.F.; Stan, G.E. Cationic substitutions in hydroxyapatite: Current status of the derived biofunctional effects and their in vitro interrogation methods. *Materials* **2018**, *11*, 2081. [CrossRef]
13. Jiang, Y.; Yuan, Z.; Huang, J. Substituted hydroxyapatite: A recent development. *Mater. Technol.* **2019**, *35*, 785–796. [CrossRef]
14. White, T.J.; Dong, Z.L. Structural derivation and crystal chemistry of apatites. *Acta Cryst.* **2003**, *59*, 1–16. [CrossRef] [PubMed]
15. Huang, Y.; Zhang, X.; Zhao, R.; Mao, H.; Yan, Y.; Pang, X. Antibacterial efficacy, corrosion resistance, and cytotoxicity studies of copper-substituted carbonated hydroxyapatite coating on titanium substrate. *J. Mater. Sci.* **2015**, *50*, 1688–1700. [CrossRef]
16. Jacobs, A.; Renaudin, G.; Forestier, C.; Nedelec, J.-M.; Descamps, S. Biological properties of copper-doped biomaterials for orthopedic applications: A review of antibacterial, angiogenic and osteogenic aspects. *Acta Biomater.* **2020**, *117*, 21–39. [CrossRef] [PubMed]
17. Kolmas, J.; Groszyk, E.; Kwiatkowska-Różycka, D. Substituted hydroxyapatites with antibacterial properties. *BioMed Res. Int.* **2014**, *2014*, 178123. [CrossRef]
18. Barralet, J.; Gbureck, U.; Habibovic, P.; Vorndran, E.; Gerard, C.; Doillon, C.J. Angiogenesis in calcium phosphate scaffolds by inorganic copper ion release. *Tissue Eng.* **2009**, *15*, 1601–1609. [CrossRef]
19. Shi, F.; Liu, Y.; Zhi, W.; Xiao, D.; Li, H.; Duan, K.; Qu, S.; Weng, J. The synergistic effect of micro/nano-structured and Cu^{2+}-doped hydroxyapatite particles to promote osteoblast viability and antibacterial activity. *Biomed. Mater.* **2017**, *12*, 035006. [CrossRef]
20. Renaudin, G.; Gomes, S.; Nedelec, J.M. First-row transition metal doping in calcium phosphate. Bioceramics: A detailed crystallographic study. *Materials* **2017**, *10*, 92. [CrossRef]
21. Gomes, S.; Vichery, C.; Descamps, S.; Martinez, H.; Kaur, A.; Jacobs, A.; Nedelec, J.M.; Renaudin, G. Cu-doping of calcium phosphate bioceramics: From mechanism to the control of cytotoxicity. *Acta Biomater.* **2018**, *65*, 462–474. [CrossRef]
22. Bhattacharjee, A.; Fang, Y.; Hooper, T.J.N.; Kelly, N.L.; Gupta, D.; Balani, K.; Manna, I.; Baikie, T.; Bishop, P.T.; White, T.J.; et al. Crystal chemistry and antibacterial properties of cupriferous hydroxyapatite. *Materials* **2019**, *12*, 1814. [CrossRef]
23. Karpov, A.S.; Nuss, J.; Jansen, M.; Kazin, P.E.; Tretyakov, Y.D. Synthesis, crystal structure and properties of calcium and barium hydroxyapatites containing copper ions in hexagonal channels. *Solid State Sci.* **2003**, *5*, 1277–1283. [CrossRef]
24. Imrie, F.E.; Skakle, J.M.S.; Gibson, I.R. Preparation of copper-doped hydroxyapatite with varying x in the composition Ca10(PO4)6CuxOyHz. *Bioceram. Dev. Appl. S* **2013**, *1*, 2013. Available online: https://www.semanticscholar.org/paper/Preparation-of-Copper-Doped-Hydroxyapatite-with-x-Imrie-Skakle/81a5134723355083919732 7f45f889e414b91754?p2df (accessed on 20 April 2023). [CrossRef]
25. Pogosova, M.A.; Provotorov, D.I.; Eliseev, A.A.; Kazin, P.E.; Jansen, M. Synthesis and characterization of the Bi-for-Ca substituted copper-based apatite pigments. *Dye. Pigment.* **2015**, *113*, 96–101. [CrossRef]
26. Othmani, M.; Bachoua, H.; Ghandour, Y.; Aissa, A.; Debbabi, M. Synthesis, characterization and catalytic properties of copper-substituted hydroxyapatite nanocrystals. *Mater. Res. Bull.* **2018**, *97*, 560–566. [CrossRef]
27. Bulina, N.; Vinokurova, O.; Eremina, N.; Prosanov, I.; Khusnutdinov, V.; Chaikina, M. Features of solid-phase mechanochemical synthesis of hydroxyapatite doped by copper and zinc ions. *J. Solid State Chem.* **2021**, *296*. [CrossRef]
28. Chaikina, M.V.; Bulina, N.V.; Prosanov, I.Y.; Vinokurova, O.B.; Ischenko, A.V. Structure formation of zinc-substituted hydroxyapatite during mechanochemical synthesis. *Inorg. Mater.* **2020**, *56*, 402–408. [CrossRef]
29. Avvakumov, E.G.; Potkin, A.R.; Samarin, O.I. Planetary Mill. USSR Patent 975068, 26 June 1981.
30. Rietveld, H.M. A Profile Refinement Method for Nuclear and Magnetic Structures. *J. Appl. Cryst.* **1969**, *2*, 65–70. [CrossRef]
31. Chaikina, M.V.; Bulina, N.V.; Vinokurova, O.B.; Gerasimov, K.B.; Prosanov, I.Y.; Kompankov, N.B.; Lapina, O.B.; Papulovskiy, E.S.; Ischenko, A.V.; Makarova, S.V. Possibilities of mechanochemical synthesis of apatites with different Ca/P ratios. *Ceramics* **2022**, *5*, 404–422. [CrossRef]
32. Chaikina, M.V.; Bulina, N.V.; Vinokurova, O.B.; Prosanov, I.Y.; Dudina, D.V. Interaction of calcium phosphates with calcium oxide or calcium hydroxide during the "soft" mechanochemical synthesis of hydroxyapatite. *Ceram. Int.* **2019**, *45*, 16927–16933. [CrossRef]
33. Sutter, B.; Wasowicz, T.; Howard, T.; Hossner, L.R.; Ming, D.W. Characterization of iron, manganese, and copper synthetic hydroxyapatites by electron paramagnetic resonance spectroscopy. *Soil Sci. Soc. Am. J.* **2002**, *66*, 1359–1366. [CrossRef]
34. Bulina, N.V.; Eremina, N.V.; Vinokurova, O.B.; Ishchenko, A.V.; Chaikina, M.V. Diffusion of copper ions in the lattice of substituted hydroxyapatite during heat treatment. *Materials* **2022**, *15*, 5759. [CrossRef]
35. Ruszala, F.A.; Kostiner, E. The hydrothermal synthesis and crystal growth of various whitlockites and a manganese containing graftonite. *J. Cryst. Growth* **1980**, *48*, 473–474. [CrossRef]
36. Bulina, N.V.; Chaikina, M.V.; Prosanov, I.Y. Mechanochemical synthesis of Sr-substituted hydroxyapatite. *Inorg. Mater.* **2018**, *54*, 820–825. [CrossRef]
37. Chaair, H.; Labjar, H.; Britel, O. Synthesis of β-tricalcium phosphate. *Morphologie* **2017**, *101*, 120–124. [CrossRef] [PubMed]

38. Berzina-Cimdina, L.; Borodajenko, N. Research of calcium phosphates using fourier transform infrared spectroscopy. *Infrared Spectrosc.* **2012**. [CrossRef]
39. Tõnsuaadu, K.; Gross, K.A.; Plūduma, L.; Veiderma, M. A review on the thermal stability of calcium apatites. *J. Therm. Anal. Calorim.* **2012**, *110*, 647–659. [CrossRef]